

# Multi-subject Task-related fMRI Data Analysis via Generalized Canonical Correlation Analysis\*

Paris A. Karakasis, *Student Member, IEEE*<sup>1</sup>, Athanasios P. Liavas, *Member, IEEE*<sup>2</sup>,  
Nicholas D. Sidiropoulos, *Fellow, IEEE*<sup>3</sup>, Panagiotis G. Simos<sup>4</sup>, and Efrosyni Papadaki<sup>5</sup>

**Abstract**—Functional magnetic resonance imaging (fMRI) is one of the most popular methods for studying the human brain. It measures brain activity, by detecting local changes of Blood Oxygen Level Dependent (BOLD) signal in the brain, over time, and can be used in both task-related and resting-state studies. In task-related studies, our aim is to determine which brain areas are activated when a specific task is performed. Various unsupervised multivariate statistical methods are being increasingly employed in fMRI data analysis. Their main goal is to extract information from a dataset, often with no prior knowledge of the experimental conditions. Generalized canonical correlation analysis (gCCA) is a well known statistical method that can be considered as a way to estimate a linear subspace, which is “common” to multiple random linear subspaces. We propose a new fMRI data generating model which takes into consideration the existence of common task-related and resting-state components. We estimate the common spatial task-related component via a two-stage gCCA. We test our theoretical results using real-world fMRI data. Our experimental findings corroborate our theoretical results, rendering our approach a very good candidate for multi-subject task-related fMRI processing.

**Clinical relevance**— This work provides a set of methods for amplifying and recovering commonalities across subjects that appear in data from multi-subject task-related fMRI experiments.

## I. INTRODUCTION

Functional magnetic resonance imaging (fMRI) is one of the most popular methods for studying the human brain. It provides a non-invasive way to measure brain activity, by detecting local changes of Blood Oxygen Level Dependent (BOLD) signal in the brain, over time. The purpose of task-based fMRI data analysis is to determine which brain areas

<sup>1</sup> P. A. Karakasis was with the School of Electrical and Computer Engineering, Technical University of Crete, Crete, Greece. He is now with the Department of Electrical and Computer Engineering, University of Virginia, Charlottesville, VA 22904, pk4cf@virginia.edu.

<sup>2</sup> A. P. Liavas is with the School of Electrical and Computer Engineering, Technical University of Crete, Crete, Greece, liavas@telecom.tuc.gr.

<sup>3</sup> N. D. Sidiropoulos is with the Department of Electrical and Computer Engineering, University of Virginia, Charlottesville, VA 22904, nikos@virginia.edu.

<sup>4,5</sup> P. G. Simos and E. Papadaki are with the School of Medicine, University of Crete, Crete, Greece, akis.simos@gmail.com, fpapada@otenet.gr.

\* P. A. Karakasis, A. P. Liavas, P. G. Simos, and E. Papadaki were partially supported by the European Regional Development Fund of the European Union and Greek national funds through the Operational Program Competitiveness, Entrepreneurship, and Innovation, under the call RESEARCH - CREATE - INNOVATE (project code : T1EDK-03360).

<sup>5</sup> N. D. Sidiropoulos was supported in part by NSF ECCS-1807660, and NSF IIS-1704074.

are activated when a specific task is performed. Hence, brain activation maps related to specific tasks can be obtained. This procedure is very useful for understanding how the human brain is functioning.

Spontaneous modulation of the BOLD signal, which cannot be attributed to the experimental paradigm or any other explicit input or output, is also present and is usually viewed as “noise” in task-related studies [1], [2]. However, in addition to physiological and magnetic noise, background BOLD signal reflects systematic fluctuations in regional brain activity. In particular, BOLD fluctuations are correlated between functionally related brain regions, forming resting-state brain networks. Moreover, this baseline activity continues during task performance, showing a similar neuro-anatomical distribution to that observed at rest [3–6], while there are studies suggesting that measured neuronal responses represent an approximately linear superposition of task-evoked neuronal activity and ongoing spontaneous activity [3].

Canonical correlation analysis (CCA) is a well known statistical method, developed by Hotelling in 1936 [7]. It can be seen as a method for the computation of basis vectors for two sets of random variables (i.e., two random vectors) such that the correlation between the respective projections of the random variables onto these basis vectors is maximized [8]. After considering the subspace that is spanned from such a set of basis vectors, CCA can be also considered as a method for the estimation of a linear subspace which is “common” to these sets of random variables [9].

Generalization of CCA to more than two random vectors dates back to [10–14]. Kettenring proposed five different formulations of the generalized CCA (gCCA) problem in [15]; all of them are equivalent to the classical CCA when the number of random vectors is two [16]. Among the different formulations of gCCA, the MAX-VAR formulation has attracted particular attention, since it enjoys a simple solution via eigen-decomposition, while scalable and structure promoting iterative algorithms for two of the gCCA formulations, MAX-VAR and SUM-COR, have been proposed in [17–19].

## A. Problem Definition

We focus on the case where the task-related fMRI experiment of a session consists of only one type of stimulus. Our aim is to determine which brain areas are activated when the stimulus is applied and construct the associated brain activation maps.

## B. Related Work

CCA and constrained CCA based methods have been applied to local voxel neighborhoods to obtain adaptive subject-specific spatial filter kernels for noise reduction purposes [20–23]. In [24], the authors used gCCA to separate different temporal sources in fMRI data. They assumed that there are some common temporal responses to external stimulation in the subjects being studied, which may be explored using gCCA. In contrast, in [25], the underlying assumption is that there are multiple subjects that share an unknown spatial response (or spatial map) to the common experimental excitation but may show different temporal responses to external stimulation. In addition, estimating “common” subspaces from multiple datasets, via CCA and gCCA based methods, has been considered in [9], [26].

## C. Our Contribution

We adopt the assumptions of [25], with respect to the common spatial maps, and assume the existence of one common temporal component, which is related to the common experimental excitation. We propose a new data generating model which takes into consideration both the common task-related and resting-state spatial components. We use gCCA and estimate the subspace that is spanned by the common spatial components. Based on this estimate, we compute the common task-related time component, using, again, gCCA. Finally, we use the estimated common task-related time component to derive an estimate of the associated common task-related spatial component and construct the respective activation map.

We test our theoretical results using real-world fMRI data. We observe that our experimental findings corroborate our theoretical results, rendering our approach a very good candidate for multi-subject task-related fMRI processing.

## D. Notation

Scalars are denoted by small letters, vectors by small bold letters, and matrices by capital bold letters, for example,  $x$ ,  $\mathbf{x}$ ,  $\mathbf{X}$ . Sets are denoted by blackboard bold capital letters, for example,  $\mathbb{U}$ .  $\mathbb{R}$  denotes the sets of real numbers.  $\mathbb{R}^{I \times J}$  denotes the set of  $(I \times J)$  real matrices. Inequality  $\mathbf{X} \geq \mathbf{0}$  means that matrix  $\mathbf{X}$  has nonnegative elements and  $\mathbb{R}_+^{I \times J}$  denotes the set of  $(I \times J)$  real matrices with nonnegative elements.  $\|\mathbf{x}\|_2$  denotes the Euclidean norm of vector  $\mathbf{x}$ , while  $\|\mathbf{X}\|_2$  and  $\|\mathbf{X}\|_F$  denote, respectively, the spectral and the Frobenius norm of matrix  $\mathbf{X}$ . The transpose and the pseudoinverse of matrix  $\mathbf{X}$  are denoted, respectively, by  $\mathbf{X}^T$  and  $\mathbf{X}^\dagger$ . The linear space spanned by the columns of matrix  $\mathbf{X}$  is denoted by  $\text{col}(\mathbf{X})$ . The orthogonal projection onto a linear subspace  $\mathcal{S}$  is denoted by  $\mathbf{P}_{\mathcal{S}}$ . The element-wise projection onto the nonnegative real numbers of vector  $\mathbf{x}$  is denoted by  $(\mathbf{x})_+$ . Finally, we use the Matlab style expressions  $\mathbf{X}(:, l)$  and  $\mathbf{X}(k, :)$ , which denote, respectively, the  $l$ -th column and the  $k$ -th row of matrix  $\mathbf{X}$ .

## II. DATA MODEL

Let  $\{\mathbf{X}_k\}_{k=1}^K$  be a set of matrices, where  $\mathbf{X}_k \in \mathbb{R}^{N \times M}$  denotes the data of the  $k$ -th subject,  $N$  denotes the number of voxels, and  $M$  denotes the number of time points (note that, in general,  $N \gg M$ ). Let  $R$  be a positive integer smaller than  $M$ . For each matrix  $\mathbf{X}_k$ , for  $k = 1, \dots, K$ , we adopt the model

$$\mathbf{X}_k = \lambda_k \mathbf{a} \mathbf{s}^T + \mathbf{A} \mathbf{S}_k^T + \mathbf{E}_k, \quad (1)$$

where:

- 1)  $\mathbf{a} \in \mathbb{R}_+^N$  and  $\mathbf{s} \in \mathbb{R}^M$  denote, respectively, the common, to all subjects, task-related spatial and temporal component, and  $\lambda_k \in \mathbb{R}_+$  denotes the intensity of the common rank-one term for the  $k$ -th subject;
- 2)  $\mathbf{A} \in \mathbb{R}_+^{N \times (R-1)}$ , whose columns are the common, to all subjects, spatial components related with the spontaneous fMRI activity;
- 3)  $\mathbf{S}_k \in \mathbb{R}^{M \times (R-1)}$ , whose columns are the temporal components, which are associated with the spontaneous fMRI activity and, in general, vary across subjects. Moreover, we assume that

$$\bigcap_{k=1}^K \text{col}(\mathbf{S}_k) = \emptyset, \quad (2)$$

that is, there is no subspace that is common to *all*  $\text{col}(\mathbf{S}_k)$ , for  $k \in \{1, \dots, K\}$ ;

- 4)  $\mathbf{E}_k \in \mathbb{R}^{N \times M}$  denotes the “unmodelled fMRI signal” of the  $k$ -th subject and can be considered as (strong) additive noise. We assume that terms  $\mathbf{E}_k$  are statistically independent from each other.

We propose model (1) based on both the existing literature [1–6], [25], [27], [28] and the detailed examination of our real-world data. Our aim is to obtain an accurate estimate of the common spatial term  $\mathbf{a}$ , which will lead to a precise activation brain map and, by extension, to the localization of the stimulated brain areas.

In order to use simpler notation, we define the matrix of the common spatial components

$$\mathbf{W} := [\mathbf{a} \ \mathbf{A}] \in \mathbb{R}_+^{N \times R}, \quad (3)$$

and the matrices of the temporal components

$$\mathbf{Z}_k := [\lambda_k \mathbf{s} \ \mathbf{S}_k] \in \mathbb{R}^{M \times R}, \quad \text{for } k = 1, \dots, K. \quad (4)$$

We further assume that matrices  $\mathbf{W}$  and  $\mathbf{Z}_k$ , for  $k = 1, \dots, K$ , are full-column rank. Using this notation, matrix  $\mathbf{X}_k$ , defined in (1), can be expressed as

$$\mathbf{X}_k = \mathbf{W} \mathbf{Z}_k^T + \mathbf{E}_k. \quad (5)$$

## III. METHODS

In this section, we describe our approach for the estimation of the common spatial factor  $\mathbf{a}$ , which consists of three stages:

- 1) we use  $\mathbf{X}_k$ , for  $k = 1, \dots, K$ , and obtain an orthonormal basis for an estimate of the common spatial subspace,  $\text{col}(\mathbf{W})$ , by solving a gCCA problem;

- 2) using the solution of the first stage, we obtain an estimate of the unique common time component  $\mathbf{s}$ , by solving a second gCCA problem;
- 3) using the estimate of  $\mathbf{s}$ , we obtain an estimate of  $\mathbf{a}$ .

#### A. Common Spatial Subspace Estimation via gCCA

We assume that the dimension,  $R$ , of the common spatial subspace,  $\text{col}(\mathbf{W})$ , is known. In order to estimate an orthonormal basis for  $\text{col}(\mathbf{W})$ , we solve the following optimization problem, which arises from the MAXVAR formulation of the gCCA [12]

$$\begin{aligned} \min_{\{\mathbf{Q}_k\}_{k=1}^K, \mathbf{G}} \sum_{k=1}^K \|\mathbf{X}_k \mathbf{Q}_k - \mathbf{G}\|_F^2 \\ \text{s.t. } \mathbf{G}^T \mathbf{G} = \mathbf{I}_R, \end{aligned} \quad (6)$$

where  $\mathbf{Q}_k \in \mathbb{R}^{M \times R}$ , for  $k = 1, \dots, K$ , and  $\mathbf{G} \in \mathbb{R}^{N \times R}$ .

The solution  $\mathbf{Q}_k^o$ , for  $k = 1, \dots, K$ , and  $\mathbf{G}^o$  of problem (6) can be computed as follows. For a fixed  $\mathbf{G}$ , the optimal  $\mathbf{Q}_k$  can be expressed as  $\mathbf{Q}_k(\mathbf{G}) = \mathbf{X}_k^\dagger \mathbf{G}$ , for  $k = 1, \dots, K$ . If we substitute this expression into (6), then the problem becomes

$$\max_{\mathbf{G}^T \mathbf{G} = \mathbf{I}_R} \text{Tr} \left( \mathbf{G}^T \left( \sum_{k=1}^K \mathbf{X}_k \mathbf{X}_k^\dagger \right) \mathbf{G} \right). \quad (7)$$

If we define

$$\mathbf{M} := \sum_{k=1}^K \mathbf{X}_k \mathbf{X}_k^\dagger, \quad (8)$$

with eigenvalue decomposition given by

$$\mathbf{M} = \mathbf{U}_M \mathbf{\Lambda}_M \mathbf{U}_M^T, \quad (9)$$

then an optimal solution  $\mathbf{G}^o$  is given by [18]

$$\mathbf{G}^o = \mathbf{U}_M(:, 1 : R). \quad (10)$$

If the fMRI data matrices  $\mathbf{X}_k$  were noiseless, in the sense that  $\mathbf{E}_k = \mathbf{0}$ , for  $k = 1, \dots, K$ , then the solution of problem (6) would result to  $\mathbf{G}^o$ , such that (see (5))

$$\text{col}(\mathbf{G}^o) = \text{col}(\mathbf{W}). \quad (11)$$

Furthermore, in this case and for all  $k \in \{1, \dots, K\}$ , matrices  $\mathbf{Q}_k^o$  and  $\mathbf{Z}_k$  would span the same subspace, namely

$$\text{col}(\mathbf{Q}_k^o) = \text{col}(\mathbf{Z}_k). \quad (12)$$

This holds because, if  $\mathbf{W} = \mathbf{G}^o \mathbf{P}$ , then

$$\mathbf{Q}_k^o = \mathbf{X}_k^\dagger \mathbf{G}^o = (\mathbf{Z}_k^T)^\dagger \mathbf{W}^\dagger \mathbf{G}^o = \mathbf{Z}_k \mathbf{F},$$

where  $\mathbf{F} := (\mathbf{Z}_k^T \mathbf{Z}_k)^{-1} \mathbf{P}^{-1}$ . The fact that  $\mathbf{E}_k$ , for  $k = 1, \dots, K$ , are nonzero makes (11) and (12) approximate and not exact equalities.

In the sequel, we shall compute an estimate of  $\mathbf{s}$  by assuming that (12) is exact. We shall check the accuracy of our arguments and the effectiveness of our approach in the section with the experimental results.

#### B. Common Time Component Extraction

Based on assumption (2) and definition (4), we have that, in the noiseless case,

$$\bigcap_{k=1}^K \text{col}(\mathbf{Z}_k) = \text{col}(\mathbf{s}), \quad (13)$$

which, using (12), leads to

$$\bigcap_{k=1}^K \text{col}(\mathbf{Q}_k^o) = \text{col}(\mathbf{s}). \quad (14)$$

We obtain an estimate of  $\mathbf{s}$  by solving the following MAXVAR problem

$$\begin{aligned} \min_{\{\mathbf{d}_k\}_{k=1}^K, \mathbf{g}} \sum_{k=1}^K \|\mathbf{Q}_k^o \mathbf{d}_k - \mathbf{g}\|_2^2 \\ \text{s.t. } \|\mathbf{g}\|_2 = 1. \end{aligned} \quad (15)$$

If we denote the optimal  $\mathbf{g}$  in (15) by  $\mathbf{g}^o$ , we have that

$$\mathbf{g}^o = \pm \frac{\mathbf{s}}{\|\mathbf{s}\|_2}. \quad (16)$$

Since (12) defines a family of approximate equalities, equality (14) and, therefore, (16) are approximate.

#### C. Estimation of the common spatial component $\mathbf{a}$

Having obtained the estimate  $\mathbf{g}^o$  of the common temporal component,  $\mathbf{s}$ , we can estimate the common spatial component,  $\mathbf{a}$ , by using various approaches. In the sequel, we present a simple approach. A more extensive treatment will appear in [29].

First, we consider the problem

$$\begin{aligned} \min_{\lambda \geq 0} \sum_{k=1}^K \|\mathbf{X}_k - \lambda_k \mathbf{a} \mathbf{g}^{oT}\|_F^2 \\ \text{s.t. } \mathbf{a} \in \text{col}(\mathbf{G}^o). \end{aligned} \quad (17)$$

Let  $\mathbf{X}_k^o := \mathbf{P}_{\text{col}(\mathbf{G}^o)} \mathbf{X}_k$ , for  $k = 1, \dots, K$ , denote the data matrices after projection onto the subspace spanned by the columns of  $\mathbf{G}^o$ . The projection of the fMRI data onto the common spatial subspace has a significant noise reduction effect. Then, one can easily show that the optimization problem (17) is equivalent to the problem

$$\min_{\lambda \geq 0} \sum_{k=1}^K \|\mathbf{X}_k^o - \lambda_k \mathbf{a} \mathbf{g}^{oT}\|_F^2. \quad (18)$$

Finally, if we add nonnegativity constraints on the elements of  $\mathbf{a}$ , we obtain the problem

$$\min_{\mathbf{a} \geq 0, \lambda \geq 0} \sum_{k=1}^K \|\mathbf{X}_k^o - \lambda_k \mathbf{a} \mathbf{g}^{oT}\|_F^2, \quad (19)$$

whose solution  $(\mathbf{a}^o, \boldsymbol{\lambda}^o)$  is an estimate of the common spatial component  $\mathbf{a}$  and the corresponding vector of intensities  $\boldsymbol{\lambda}$ .

#### IV. EXPERIMENTS

In this section, we test our approach using real-world task-related fMRI data. Specifically, we process four datasets, recorded at the University of Crete General Hospital, from a group of 25 healthy adults, performing four visual tasks which were identical in either the precise kinematics of an observed person-directed action or the target of an action (executed toward a person or an inanimate object) with the same kinematics. First, we quote some information regarding the experiment design and the preprocessing pipeline that was applied to the data and, then, we present the results obtained by analyzing the data using our method.

##### A. Experiment design

The fMRI block design consists of four action observation conditions, each involving four “active” 35 sec blocks alternating with four 35 sec baseline blocks. Indicative specifications are presented below. A video clip illustrating a two-movement action sequence was presented 6 times within each “active” block. The stimulus set-up was identical across blocks and conditions, consisting of a fixed red spot at the center of the display, presenting a female person sitting behind a table, presenting a female person sitting behind a table. A white tea cup was positioned on the table and a ceramic bowl 30 cm in diameter was located on a smaller table right next to the person’s head.

The data employed in the main analyses reported here were derived from the first of the four experimental conditions, examining the effects of an action with the same goal but different kinematics.<sup>1</sup> More specifically, the “Fast to cup – Slow to person” condition (or, briefly, condition (i)) consists of a rapid grasping movement toward the tea cup (time duration equal to 1400 ms and average velocity equal to 0.36 m/sec), followed by a much slower movement that brings the cup to the person’s mouth (time duration equal to 4038 ms and average velocity equal to 0.12 m/sec).

##### B. Image acquisition and pre-processing

Scanning was performed on an upgraded 1.5 T Siemens Vision/Sonata scanner (Erlangen, Germany) with powerful gradients (Gradient strength: 45 mT/m, Gradient slew rate: 200 mT/m/ms) and a standard four channel head array coil. For the BOLD-fMRI, a  $T2^*$ -weighted, fat-saturated 2D-FID-EPI sequence was used with the following parameters: repetition time (TR) 3500 ms, echo time (TE) 50 ms, field of view (FOV)  $192 \times 192 \times 108$  ( $x, y, z$ ), acquisition voxel size  $3 \times 3 \times 3$  mm. Whole brain scans consisted of 36 transverse slices with 3.0-mm slice thickness and no interslice gap. The time-series recorded in each condition comprised 80 volumes (time points), with 40 volumes recorded during observation of repeated person-directed action (clip duration 5438 ms) and 40 volumes recorded during observation of repeated presentation of the first frame of the video clip presented continuously for 5438 ms. In our analysis, as is customary in fMRI studies, we ignore the first 5 volumes of each time

<sup>1</sup>The results concerning the other three experimental conditions will be presented in a more extensive document [29].

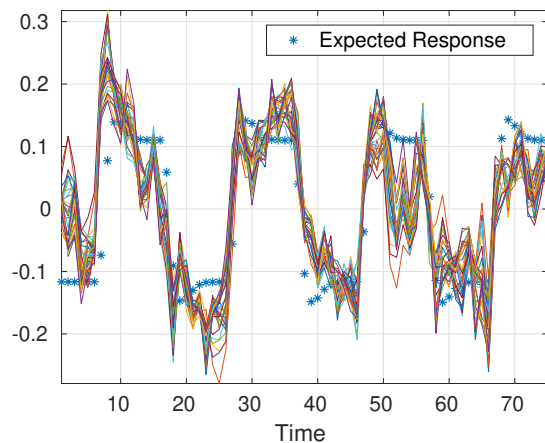


Fig. 1. Estimated  $g^o$  for varying common spatial subspace dimensions, from 10 to 40. The signal depicted with blue stars is the  $s_{exp}$ .

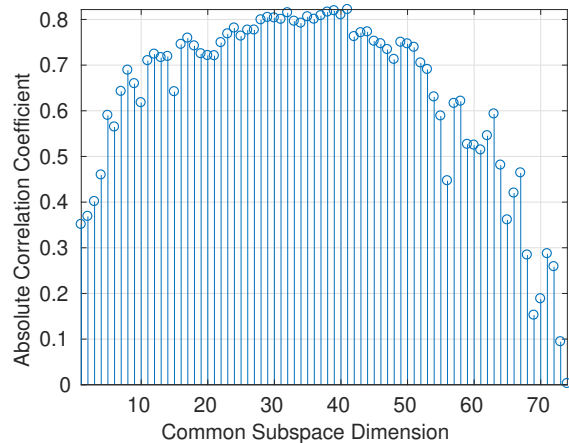


Fig. 2. Absolute correlation coefficient between  $s_{exp}$  and  $g^o$  across different common spatial subspace dimensions.

series. Additionally, high resolution anatomical images were acquired sagittally, using a 3D magnetization-prepared rapid acquisition gradient echo sequence (3D-MPRAGE) with the following parameters: TR 9.8 ms, TE 4.6 ms, flip angle 8 deg, inversion time (TI) 922 ms, FOV  $180 \times 230$  ( $x, z$ ), with acquisition voxel size of  $0.98 \times 0.98$  ( $x, z$ ) and slice thickness of 1 mm.

Image preprocessing was performed in SPM8.<sup>2</sup> Initially, EPI scans were spatially realigned to the first image of the first time-series using second-degree B-spline interpolation algorithms and motion-corrected through rigid body transformations (three translations and three rotations about each axis). Next, images were spatially normalized to a common brain space (MNI template) and smoothed using an isotropic Gaussian filter (FWHM=8 mm). At last, all voxel time-series were centered (subtraction of the mean value over time).

We note that the SPM platform is able to provide a time response component, based on the activation onsets and offsets, which is expected to appear in the activated brain voxels. We denote this response as  $s_{exp}$ .

<sup>2</sup>Statistical Parametric Mapping software, SPM: Welcome Department of Imaging Neuroscience, London, UK; available at: <http://www.fil.ion.ucl.ac.uk/spm/>.

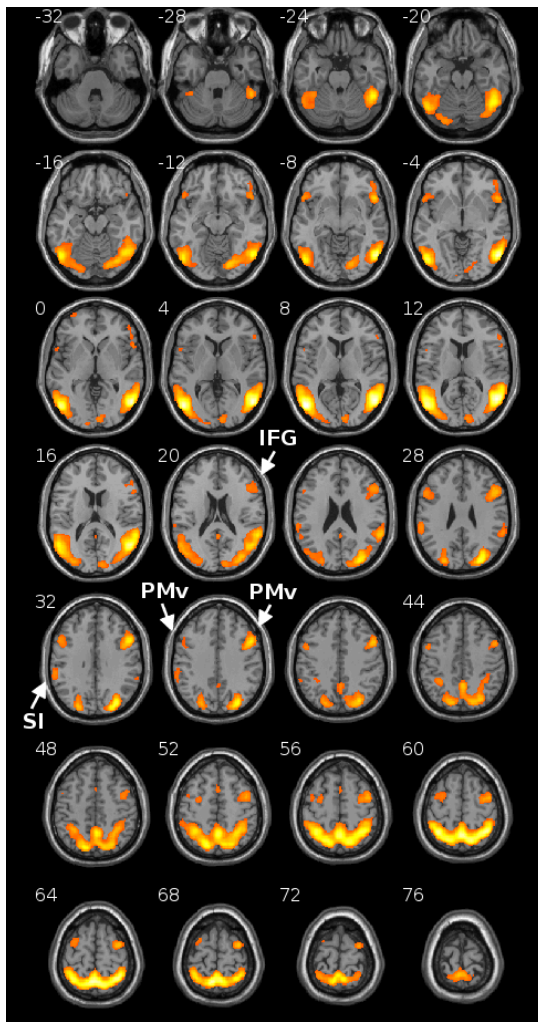


Fig. 3. Map  $\mathbf{a}^o$  calculated for common subspace dimension equal to 30. The map was thresholded such that the 10% of the voxels with the largest voxel score of  $\mathbf{a}^o$  are shown. A standard Z-transform is not meaningful, since  $\mathbf{a}^o$  satisfies nonnegativity constraints.

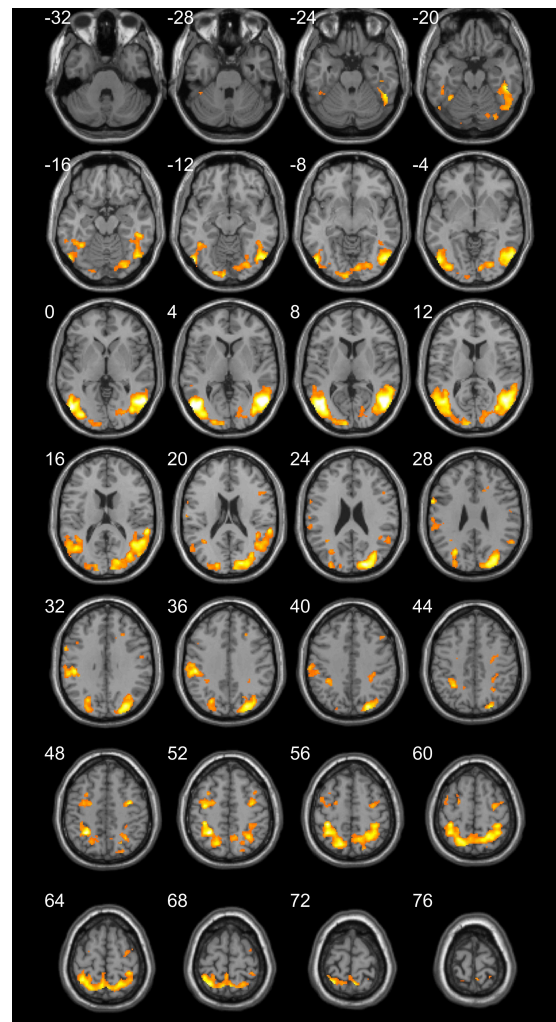


Fig. 5. Map obtained using the conventional General Linear Model with a priori knowledge of the timing of the experimental (video clip observation) and reference blocks (static hand viewing) in SPM (at a standard threshold of  $p < 0.001$  uncorrected in the 2nd level analysis).

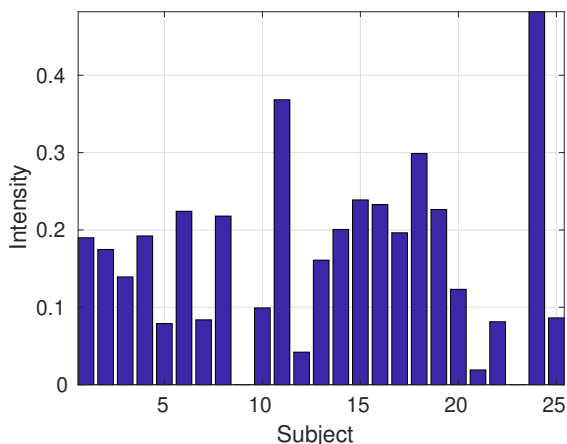


Fig. 4. Estimate  $\lambda^o$  of vector of intensities for “common” subspace dimension equal to 30.

### C. Results

Next, we present the results obtained from the data of condition (i) using our approach. In Fig. 1, we plot the estimated common temporal component,  $\mathbf{g}^o$ , which emerged for various common spatial subspace dimensions,  $R$ , as well as the normalized, to unit 2-norm, expected response  $\mathbf{s}_{\text{exp}}$ . In Fig. 2, we plot the absolute correlation coefficients between  $\mathbf{s}_{\text{exp}}$  and  $\mathbf{g}^o$ , for all possible values of  $R$ . In these figures, we observe that

- 1) the estimated  $\mathbf{g}^o$ , for different common spatial subspace dimensions, are very much alike. Thus, our method is *not* sensitive to the exact value of  $R$ , which is unknown, in general.
- 2) the estimated  $\mathbf{g}^o$  are quite similar to the expected signal  $\mathbf{s}_{\text{exp}}$ .

We conclude that our method effectively estimates the common temporal component, with *no prior* knowledge about its shape.

In Figures 3 and 4, we depict, respectively, the spatial map  $\mathbf{a}^\circ$  and the intensities  $\lambda^\circ$  that emerged from the solution of (19). To assess the anatomic sensitivity and accuracy of our method, in Fig. 5, we depict the contrast map obtained by the conventional General Linear Model with a priori knowledge of the timing of the experimental (video clip observation) and reference blocks (static hand viewing) in SPM (at a standard threshold of  $p < 0.001$  uncorrected). The juxtaposition of the two maps reveals that our method successfully captures all clusters of activation voxels in key components of the brain network putatively involved in evaluating the kinematic characteristics and intentions of the observed actions of other subjects, including the inferior frontal gyrus (IFG), ventral Premotor Area (PMv), and primary somatosensory area (SI).

## V. CONCLUSIONS

We proposed a two-stage gCCA method for single-task multi-subject fMRI analysis. Our data model successfully captures the basic features of the fMRI signal.

Due to space limitation, we did not elaborate on assumption (2) and the estimation of the common subspace dimension,  $R$ . This will be done in a more extensive manuscript [29], which will also include experiments with synthetic data, more elaborate approaches for the estimation of the common spatial component  $\mathbf{a}$ , and the results from the other experimental conditions.

## ACKNOWLEDGMENT

The authors would like to thank Dr. Eleutherios Kavroulakis for the help he provided with data preprocessing and Prof. Michalis Zervakis for his useful comments.

## REFERENCES

- [1] M. D. Fox and M. E. Raichle, "Spontaneous fluctuations in brain activity observed with functional magnetic resonance imaging," *Nature reviews neuroscience*, vol. 8, no. 9, p. 700, 2007.
- [2] D. A. Fair, B. L. Schlaggar, A. L. Cohen, F. M. Miezin, N. U. Dosenbach, K. K. Wenger, M. D. Fox, A. Z. Snyder, M. E. Raichle, and S. E. Petersen, "A method for using blocked and event-related fMRI data to study resting state functional connectivity," *NeuroImage*, vol. 35, no. 1, pp. 396–405, 2007.
- [3] M. D. Fox, A. Z. Snyder, J. M. Zacks, and M. E. Raichle, "Coherent spontaneous activity accounts for trial-to-trial variability in human evoked brain responses," *Nature neuroscience*, vol. 9, no. 1, p. 23, 2006.
- [4] M. D. Greicius and V. Menon, "Default-mode activity during a passive sensory task: uncoupled from deactivation but impacting activation," *Journal of cognitive neuroscience*, vol. 16, no. 9, pp. 1484–1492, 2004.
- [5] K. Arfanakis, D. Cordes, V. M. Haughton, C. H. Moritz, M. A. Quigley, and M. E. Meyerand, "Combining independent component analysis and correlation analysis to probe interregional connectivity in fMRI task activation datasets," *Magnetic resonance imaging*, vol. 18, no. 8, pp. 921–930, 2000.
- [6] P. Fransson, "How default is the default mode of brain function?: Further evidence from intrinsic BOLD signal fluctuations," *Neuropsychologia*, vol. 44, no. 14, pp. 2836–2845, 2006.
- [7] H. Hotelling, "Relations between two sets of variates," *Biometrika*, vol. 28, no. 3–4, pp. 321–377, 1936.
- [8] D. R. Hardoon, S. Szedmak, and J. Shawe-Taylor, "Canonical correlation analysis: An overview with application to learning methods," *Neural computation*, vol. 16, no. 12, pp. 2639–2664, 2004.
- [9] M. S. Ibrahim and N. D. Sidiropoulos, "Cell-edge interferometry: Reliable detection of unknown cell-edge users via canonical correlation analysis," in *2019 IEEE 20th International Workshop on Signal Processing Advances in Wireless Communications (SPAWC)*. IEEE, 2019, pp. 1–5.
- [10] B. Vinograd, "Canonical positive definite matrices under internal linear transformations," *Proceedings of the American Mathematical Society*, vol. 1, no. 2, pp. 159–161, 1950.
- [11] R. G. Steel *et al.*, "Minimum generalized variance for a set of linear functions," *The Annals of Mathematical Statistics*, vol. 22, no. 3, pp. 456–460, 1951.
- [12] P. Horst, "Generalized canonical correlations and their applications to experimental data," *Journal of Clinical Psychology*, vol. 17, no. 4, pp. 331–347, 1961.
- [13] —, "Relations among  $m$  sets of measures," *Psychometrika*, vol. 26, no. 2, pp. 129–149, 1961.
- [14] J. D. Carroll, "Generalization of canonical correlation analysis to three or more sets of variables," in *Proceedings of the 76th annual convention of the American Psychological Association*, vol. 3, 1968, pp. 227–228.
- [15] J. R. Kettenring, "Canonical analysis of several sets of variables," *Biometrika*, vol. 58, no. 3, pp. 433–451, 1971.
- [16] N. A. Asendorf, "Informative data fusion: Beyond canonical correlation analysis," 2015.
- [17] X. Fu, K. Huang, E. E. Papalexakis, H.-A. Song, P. P. Talukdar, N. D. Sidiropoulos, C. Faloutsos, and T. Mitchell, "Efficient and distributed algorithms for large-scale generalized canonical correlations analysis," in *2016 IEEE 16th international conference on data mining (ICDM)*. IEEE, 2016, pp. 871–876.
- [18] X. Fu, K. Huang, M. Hong, N. D. Sidiropoulos, and A. M.-C. So, "Scalable and flexible multiview MAX-VAR canonical correlation analysis," *IEEE Transactions on Signal Processing*, vol. 65, no. 16, pp. 4150–4165, 2017.
- [19] C. I. Kanatsoulis, X. Fu, N. D. Sidiropoulos, and M. Hong, "Structured SUMCOR multiview canonical correlation analysis for large-scale data," *IEEE Transactions on Signal Processing*, vol. 67, no. 2, pp. 306–319, 2018.
- [20] O. Friman, J. Cedefamn, P. Lundberg, M. Borga, and H. Knutsson, "Detection of neural activity in functional MRI using canonical correlation analysis," *Magnetic Resonance in Medicine: An Official Journal of the International Society for Magnetic Resonance in Medicine*, vol. 45, no. 2, pp. 323–330, 2001.
- [21] X. Zhuang, Z. Yang, K. R. Sreenivasan, V. R. Mishra, T. Curran, R. Nandy, and D. Cordes, "Multivariate group-level analysis for task fMRI data with canonical correlation analysis," *NeuroImage*, vol. 194, pp. 25–41, 2019.
- [22] Z. Yang, X. Zhuang, K. Sreenivasan, V. Mishra, T. Curran, R. Byrd, R. Nandy, and D. Cordes, "3D spatially-adaptive canonical correlation analysis: Local and global methods," *NeuroImage*, vol. 169, pp. 240–255, 2018.
- [23] X. Zhuang, Z. Yang, T. Curran, R. Byrd, R. Nandy, and D. Cordes, "A family of locally constrained CCA models for detecting activation patterns in fMRI," *NeuroImage*, vol. 149, pp. 63–84, 2017.
- [24] Y.-O. Li, W. Wang, T. Adali, and V. D. Calhoun, "CCA for joint blind source separation of multiple datasets with application to group fMRI analysis," in *2008 IEEE International Conference on Acoustics, Speech and Signal Processing*. IEEE, 2008, pp. 1837–1840.
- [25] B. Afshin-Pour, G.-A. Hossein-Zadeh, S. C. Strother, and H. Soltanian-Zadeh, "Enhancing reproducibility of fMRI statistical maps using generalized canonical correlation analysis in NPAIRS framework," *NeuroImage*, vol. 60, no. 4, pp. 1970–1981, 2012.
- [26] G. Zhou, A. Cichocki, Y. Zhang, and D. P. Mandic, "Group component analysis for multiblock data: Common and individual feature extraction," *IEEE transactions on neural networks and learning systems*, vol. 27, no. 11, pp. 2426–2439, 2015.
- [27] E. B. Erhardt, S. Rachakonda, E. J. Bedrick, E. A. Allen, T. Adali, and V. D. Calhoun, "Comparison of multi-subject ICA methods for analysis of fMRI data," *Human brain mapping*, vol. 32, no. 12, pp. 2075–2095, 2011.
- [28] V. Calhoun, T. Adali, G. Pearlson, and J. Pekar, "Spatial and temporal independent component analysis of functional MRI data containing a pair of task-related waveforms," *Human brain mapping*, vol. 13, no. 1, pp. 43–53, 2001.
- [29] P. A. Karakasis, A. P. Liavas, N. D. Sidiropoulos, P. G. Simos, and E. Papadaki, "Multi-subject task-related fMRI data analysis via a two-stage generalized canonical correlation analysis," *in preparation*.